ELSEVIER

Journal of Cleaner Production

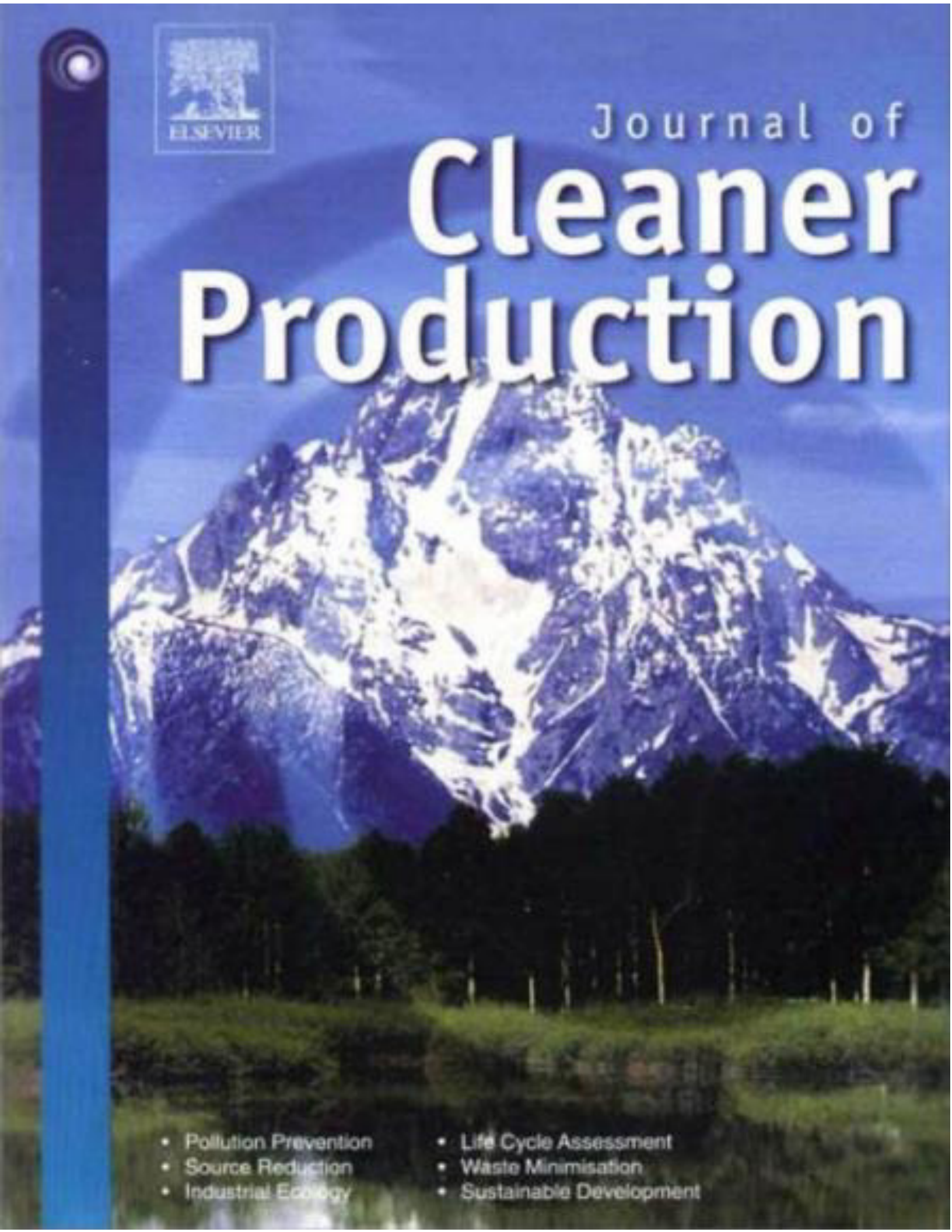

- Pollution Prevention
- Source Reduction
- Industrial Ecology
- Life Cycle Assessment
- Waste Minimisation
- Sustainable Development

ScienceDirect

Keywords

Author name

Journal of Cleaner Production

Volume

Issue

Pages

Journal of Cleaner Production

SUPPORTS OPEN ACCESS

Articles in press Latest issue Special issues All issues Sign in to set up alerts

Volume 183

Pages 1-1336 (10 May 2018)

Previous vol/issue Next vol/issue

Show all article previews Download PDFs Export

Download PDF Article preview

Research article • Full text access

Identifying the impacts of human capital on carbon emissions in Pakistan

Sadia Bano, Yuhuan Zhao, Ashfaq Ahmad, Song Wang, Ya Liu

Pages 1082-1092

Download PDF Article preview

Research article • Full text access

Modeling human activity in Spain for different economic sectors: The potential link between occupancy and energy usage

E.J. Palacios-García, A. Moreno-Munoz, I. Santiago, J.M. Flores-Arias, ... I.M. Moreno-Garcia

Pages 1093-1109

Download PDF Article preview

Research article • Full text access

A high temporal-spatial resolution air pollutant emission inventory for agricultural machinery in China

Jianlei Lang, Jingjing Tian, Ying Zhou, Kanghong Li, ... Shuiyuan Cheng

Pages 1110-1121

Download PDF Article preview

Research article • Full text access

The potential of energy savings and the prospects of cleaner energy production by solar energy integration in the residential buildings of Saudi Arabia

Hafiz M. Abd-ur-Rehman, Fahad A. Al-Sulaiman, Aamir Mehmood, Sehar Shakir, Muhammad Umer

Pages 1122-1130

Download PDF Article preview

Research article • Full text access

Economic assessment of hydrogen production from solar driven high-temperature steam electrolysis process

Deepak Yadav, Rangan Banerjee

Pages 1131-1155

Download PDF Article preview

page 1 of 2

ISSN: 0959-6526

Journal of Cleaner Production 183 (2018) 720–728

Contents lists available at ScienceDirect

Journal of Cleaner Production

journal homepage: www.elsevier.com/locate/jclepro

Effects of the presence of organic matter on the removal of arsenic from groundwater

Adriana Saldaña-Robles [a], Cesar E. Damian-Ascencio [b, *], Ricardo J. Guerra-Sanchez [c], Alberto L. Saldaña-Robles [a], Noe Saldaña-Robles [a], Armando Gallegos-Muñoz [b], Sergio Cano-Andrade [b]

[a] Department of Agricultural Engineering, Universidad de Guanajuato, Irapuato, GTO 36500, Mexico
[b] Department of Mechanical Engineering, Universidad de Guanajuato, Salamanca, GTO 36885, Mexico
[c] Department of Environmental Sciences, CIATEC, Leon, GTO 37545, Mexico

ARTICLE INFO

Article history:
Received 12 September 2017
Received in revised form
13 February 2018
Accepted 15 February 2018
Available online 19 February 2018

Keywords:
As(V) adsorption
Humic Acids
Fulvic Acids
Granular Ferric Hydroxide
Mini-columns

ABSTRACT

Arsenic is a natural contaminant present in groundwater mantles which, in high concentrations, causes severe health and environmental problems such as the degradation of human health and the contamination of land used for agriculture during irrigation. Understanding the process of arsenic removal from water contributes to the sustainability of regions where this problem is present. This work presents an experimental study complemented with numerical predictions of the adsorption of arsenic (As(V)) in mini-columns using Granular Ferric Hydroxide (GFH) as adsorbent. The work focuses on the effects of the presence of organic matter, i.e., humic (HA) and fulvic (FA) acids, in a water inflow that is contaminated with As(V). The treatments contain the same concentration of organic matter, the same initial concentration of As(V) of 0.8 mg L^{-1}, and the same amount of GFH of 2 g for the filters. Results show that the samples containing organic matter (HA and FA) show a lower adsorption capacity, a lower breakthrough volume, a lower pH, and a non uniform saturation of the GFH filter. The results suggest the need to include the effects of organic matter in all subsequent analyses of arsenic removal from water because organic matter is always present in real life scenarios. Also, this work provides useful information to solve the problematic of the presence of high concentrations of As(V) (greater than 50 μg L^{-1}) in the water mantles of the Bajio region of Mexico.

1. Introduction

The contamination of groundwater and soils due to arsenic is been a problem in Mexico (Wurl et al., 2014; Alarcón-Herrera et al., 2013), where the permissible level of arsenic in fresh water is been reduced from 50 μg L^{-1} to 25 μg L^{-1}. This concern has motivated diverse studies of the presence of this contaminant in groundwater in several regions such as Queretaro (Santos-Jallath et al., 2012), Baja California (Wurl et al., 2014), Hidalgo (Ongley et al., 2007; Romero et al., 2006), Guerrero (Armienta et al., 2003), San Luis Potosi (Razo et al., 2004), Yucatan (Arcega-Cabrera and Fargher, 2016), and Guanajuato (Mendoza-Amézquita et al., 2006). For the particular case of the Bajio region in Guanajuato, the contamination with arsenic is caused by mining practice (Wurl et al., 2014; Santos-Jallath et al., 2012) and industrial waste (Armienta and Segovia, 2008), where arsenate (As(V)) is the most common type of contaminant (Nguyen et al., 2011; Cullen and Reimer, 1989). Besides studying the presence of arsenic, finding methods to remove this contaminant from groundwater is also important; otherwise, problems to the population and environment (Burgess et al., 2010; Maji et al., 2008; Brammer and Ravenscroft, 2009; Masindi and Gitari, 2016) can be caused.

Among the several techniques that are used for removal of arsenic from aqueous mantles, the fixed-bed column treatment process is the preferred one because of its simplicity and robustness (Amy et al., 2005); and from among the adsorbents available (Maji et al., 2008; Nguyen et al., 2011; Amy et al., 2005; Kundu and Gupta,

* Corresponding author.
E-mail address: cesar.damian@ugto.mx (C.E. Damian-Ascencio).

https://doi.org/10.1016/j.jclepro.2018.02.161
0959-6526/

2007; Trois and Cibati, 2015; Kofa et al., 2015; Hu et al., 2015; Chu, 2014; Mehta and Chaudhari, 2015; Ghosh et al., 2014; Baig et al., 2014; Aredes et al., 2012; Bulut et al., 2014; Yin et al., 2017; Nieto-Delgado and Rangel-Mendez, 2012; Daus et al., 2004; Tresintsi et al., 2012; Iakovleva et al., 2016; Masindi and Gitari, 2016) GFH is of low cost and has good adsorption properties. However, the adsorption properties of GFH are greatly affected by the ions present in water (Nguyen et al., 2011). Among all the possible ions, dissolved organic matter is one of the most important carriers of As(V) from the soil to groundwater wells Tareq et al., 2013; Anawar et al., 2013. This natural organic matter is well represented by Humic (HA) and Fulvic (FA) acids (Tang et al., 2014) which come mainly from plants, soil humus, and industrial processes.

Since the presence of FA and HA affect the properties and surface reactivity of GFH (Genz et al., 2008) and the properties of other elements present in water (Rahman et al., 2013), several studies have been devoted to investigate these effects. Genc-Fuhrman et al. (2016) find that the adsorption of arsenic is lowered at higher pH and when HA are present. Watanabe et al. (2017) study the toxicity of water under the presence of arsenic, cobalt, and humic substances, finding that toxicity is reduced when HA are present; also, the toxicity is decreased when smaller molecules of HA are used. Fakour and Lin (2014) study the complexation of As with HA and FA finding that As(V) forms complexes with organic matter reducing the adsorption of As into the oxide-based filters. Uwamariya et al. (2015) study iron oxide-coated sand (IOCS) and granular ferric hydroxide (GFH) as adsorbents in filters to remove As(V) when FA are present in groundwater, finding that for this particular case FA do not affect the adsorption capacity of As(V). Kong et al. (2017) find that, using ferric chloride, the adsorption of As(V) is higher at equilibrium and it is reduced when HA are present. Luo et al. (2015) find that HA reduce the adsorption capacity of As(V) on ion oxides and prolong the reaction kinetics. However, all these studies analyze the effects of the presence of HA only or the presence of FA only.

To the best known of the authors, the effects of both, HA and FA, on the adsorption of arsenic into a single study has only been studied by Saldana-Robles et al. (2017) and Li et al. (2017). Li et al. (2017) study the effect of both HA and FA on the remotion of arsenic using modified granular natural siderite, finding that the kinetics of adsorption is not affected and that HA and FA inhibit the adsorption process, having the highest impact with FA. Saldana-Robles et al. (2017) also study the impact of both HA and FA on the adsorption of As(V) on GFH, finding that HA lower the rate constant, obtaining the lowest in the presence of FA. These two studies present curves for the removal kinetics at equilibrium conditions and the adsorption isotherms of As(V) only. However, more information needs to be collected, for instance, the pH of groundwater is an important factor that indicates how well the As(V) is bounded to organic matter and as a consequence, it indicates how well the As(V) is adsorbed on the GFH filters (Buschmann et al., 2006; Redman et al., 2002) .

In the present study, the arsenic adsorption capacity of GFH in the presence of organic matter (HA and FA) in mini-columns is presented. The novelty of the work is the experimental and numerical study of the effects of the presence of both, HA and FA, on the adsorption process of As(V) on GFH. The impact of the inclusion of organic matter in the adsorption process of As(V) is evaluated by constructing breakthrough, desorption, and pH curves from experiments, and numerical models (Thomas (Thomas, 1944; Ayoob et al., 2007), Belter (Chu, 2004), and Homogeneous Surface Diffusion (HSD) (Hand et al., 1984)) are used to predict these experimental results. Also, the HSD model is used to predict the concentration of arsenic in the GFH filter with respect to time.

2. Materials and methods

2.1. Rapid small scale column test and column parameters

The mini-columns used for the study are 20 mm diameter, and are filled with 2 g of GFH, resulting in a fixed-bed of 6 mm tall. The influent enters the mini-column at the top and moves down the mini-column by gravity, passing through the adsorbent (GFH), and leaving the mini-column at the bottom. The effluent is collected and its arsenic concentration is measured using the blue molybdenum method. The effluent pH is also measured using a buffer solution. The 0.66 mL min^{-1} volumetric flow rate that is forced to pass through the column contains an As(V) concentration of 0.8 mg L^{-1}. These parameters of volumetric flow rate and As(V) concentration are the result of a dimensional analysis that assure that the results of the present work are scalable to real problems at large scale applications. This influent volumetric flow rate is maintained constant throughout the experiment and is the same for the three treatments, i.e., WOM, HA, and FA.

2.2. Adsorbent and water composition

A commercial GFH that is produced from a ferric chloride solution by neutralisation and precipitation with NaOH Ghosh et al. (2014) is used in the experiments. The GFH is not synthesized at home. It consists of a ferric oxy-hydroxide with wet content and a porosity of 43–48% and 72–77%, respectively. The particle of the GFH is 0.5–1.0 mm diameter, with a specific surface area of 300 m^2 g^{-1}. Further characteristics and properties of the GFH are reported in Ghosh et al. (2014).

All chemicals used in the experiments are of analytical grade with no further purification. Distilled water is used for the preparation of all the solutions. Arsenate solutions are prepared by dissolving reagent grade $Na_2H{\cdot}AsO_4{\cdot}7H_2O$ in distilled water. Stock solutions of HA and FA are prepared by adding 1 g of the organic matter to 250 mL of distilled water. The total dissolved organic carbon (TOC) concentration is measured for each treatment. Three replicas of each treatment are analysed for statistics, and various blanks are analysed for contamination control.

2.3. Characteristics of the treatments

The three different chemical treatments are used for the experiments, and their composition are reported in Table 1. The first treatment does not contain organic matter (WOM), HA are added to the second treatment, and FA are added to the third treatment. For the second and third treatments, the As(V)-H_2O-Organic Matter solution contains 3 mg L^{-1} of TOC. All treatments are prepared using the same operating parameters. The experiments are developed at ambient conditions, i.e.,1 atm, 25 °C. Samples are collected

Table 1
Characteristics of the treatments.

Parameter	WOM	HA	FA
HA (mg TOC L^{-1})	0	3	0
FA (mg TOC L^{-1})	0	0	3
C_0 (mg L^{-1})	0.8	0.8	0.8
V_b (mL)	1.7	1.7	1.7
Q (mL min^{-1})	0.66	0.66	0.66
Particle size (mm)	0.5–1.0	0.5–1.0	0.5–1.0
m (g)	2.0	2.0	2.0
z (mm)	6.0	6.0	6.0
t_e (min)	2.61	2.61	2.61
pH	7.4	7.4	7.4
Temperature (°C)	25	25	25

at different times during the experiment until the As(V) concentration of the effluent reaches 95% of that of the influent.

2.4. Effect of pH

A pH of 7.4 for the influent is maintained by adding a buffer solution of either H_2SO_4 or NaOH at 0.1 M. The effluent pH is monitored during the entire sampling period for all treatments.

2.5. Regeneration of GFH

A regeneration of the absorbent is essential for its reuse in the removal of As(V). After the experiment is finished, the adsorbent is cleaned using 50 mL of distilled water. This process removes all the impurities present in the GFH. Subsequently, a constant flow of NaOH solution at 0.1 M is forced to pass continuously through the mini-column during three days in order to regenerate the GFH. Samples are continuously collected during this period. The regeneration efficiency is calculated as

$$\eta_{\text{reg}} = 100\,\frac{m_{\text{ad}}}{m_{\text{des}}} \tag{1}$$

where m_{ad} is the total mass of As(V) that is adsorbed at saturation, and m_{des} is the total mass of arsenic that is desorbed.

2.6. Methodology of analysis

The amount of As(V) removed by the GFH in the mini-column is determined by calculating the area under the $C(t)/C_0$ vs Bed Volume curve (or breakthrough curve). C_0 and $C(t)$ (mg L^{-1}) are the concentration of As(V) in the influent and effluent, respectively.

The mass transfer zone is defined as

$$Z_m = z\left(1 - \frac{V_r}{V_s}\right) \tag{2}$$

where z is the column height, V_r is the breakthrough volume and V_s is the saturation volume.

The total mass of As(V) stored in the column is obtained as

$$m_{\text{tot}} = C_0 V_e \tag{3}$$

where V_e is the effluent volume, defined as

$$V_e = Q\,t_s \tag{4}$$

Q is the volumetric flow of influent (mL min^{-1}), and t_s is the saturation time (min).

The percentage of arsenic removal with respect to the volumetric flow is obtained as

$$\%_R = 100\,\frac{m_{\text{ad}}}{m_{\text{tot}}} \tag{5}$$

The total mass of As(V) that is adsorbed by the GFH filter is calculated by integrating the breakthrough curve (Han et al., 2009), that is,

$$m_{\text{ad}} = C_0 \int_0^{V_s} \frac{C(t)}{C_0}\,dV \tag{6}$$

The maximum adsorption capacity of the column (mg g^{-1}) is determined as

$$q_{\max} = \frac{m_{\text{ad}}}{m_{\text{dry}}} \tag{7}$$

where m_{dry} is the dry mass of GFH in the mini-column.

Finally, the empty-bed contact time in the column is given by

$$t_e = \frac{V_b}{Q} \tag{8}$$

where V_b is the volume of the fixed bed (or bed volume). Using Eq. (8) together with $C(t)$ and C_0 is possible to determine the characteristics of the breakthrough curve.

2.7. Numerical modeling of breakthrough curves

Three models are used to predict the behavior of a breakthrough curve, i.e., Belter, Thomas, and HSD. These models combine the mathematical description of adsorption at equilibrium with the kinetics of adsorption, by applying a mass balance on a differential volume of the adsorbent.

The Belter model is given as (Chu, 2004).

$$\frac{C(t)}{C_0} = \frac{1}{2}\left[1 + \text{erf}\left(\frac{V_e - V_m}{\sqrt{2}\,\sigma V_m}\right)\right] \tag{9}$$

where erf$(\cdot)$ is the error function of $(\cdot)$, V_m is the effluent volume at which half of C_0 is obtained, and σ is the standard deviation of the linear part of the breakthrough curve. The parameters V_m and σ are obtained from experimental data.

In the Thomas model, the rate of the adsorption capacity and the adsorption gradient in the bed must be proportional to both, the adsorbate concentration existent in the fluid and the adsorption capacity, that is,

$$\frac{dq}{dt} = -k_T\,q\,C(t) \tag{10}$$

$$\frac{dC(t)}{dz} = -\frac{k_T\,q\,C(t)}{u} \tag{11}$$

where q is the adsorption capacity, u is the influent velocity, and k_T is the kinetic constant. Using Eqs. (10) and (11), the breakthrough curve is defined as

$$\ln\left(\frac{C_0}{C(t)} - 1\right) = \ln\left[e^{\left(k_T q \frac{m}{Q}\right)} - 1\right] - \frac{k_T\,C_0\,V_e}{Q} \tag{12}$$

which can be expressed in a linearized form as

$$\ln\left(\frac{C_0}{C(t)} - 1\right) = k_T\,q\,\frac{m}{Q} - \frac{k_T\,C_0\,V_e}{Q} \tag{13}$$

The Homogeneous Surface Diffusion Method solves the partial differential equations that govern both the advective transport of As(V) through the filter and the diffusion that is present in the adsorbent. In a dimensionless form, the advective transport through the filter is expressed as (Hand et al., 1984).

$$\frac{1}{D_g}\frac{\partial X}{\partial T} + \frac{\partial X}{\partial Z} + 3St(X - X^*) = 0 \tag{14}$$

where $Z = z/L$ is the dimensionless axial coordinate, $X = C(t)/C_0$ is the dimensionless liquid-phase concentration, $X^* = C(t)/C_0^*$ is the dimensionless liquid-phase concentration at the adsorbent surface, C_0^* is the concentration of arsenic at the surface.

Eq. (14) is subject to the initial conditions of zero concentration at the beginning

$$X(T=0,Z)=0 \tag{15}$$

and a constant influent concentration at the top of the adsorbent

$$X(T,Z=0)=1 \tag{16}$$

The intraparticle diffusion is governed by the diffusion equation

$$\frac{\partial Y}{\partial T}=\frac{St}{Bi}\left[\frac{1}{R^2}\frac{\partial}{\partial R}\left(R^2\frac{\partial Y}{\partial R}\right)\right] \tag{17}$$

where $Y=p/p_0$ is the dimensionless solid phase concentration, $R=r/r_p$ is the dimensionless radius, Bi is the Biot number.

Eq. (17) is subject to the boundary condition of symmetry at the center

$$\frac{\partial Y}{\partial R}|_{R=0}=0 \tag{18}$$

and the boundary condition for the particle surface

$$\frac{\partial Y}{\partial R}|_{R=1}=Bi(X-X^*) \tag{19}$$

which considers that, at the exterior of the adsorbent grain surface, the mass transported into the grain equals the mass transported through the stagnated fluid film.

The Chebyshev collocation method is employed to solve Eqs. (14) and (17). The advective transport equation (Eq. (14)) is discretised using the Gauss-Lobatto collocation. The system of coupled partial differential equations is reduced to a system of time-dependent ordinary differential equations that is solved using the Adams method. The St, Bi and D_g are adjusted to match the experimental results. The error of the HSD model is measured using the sum square error, defined as

$$\Gamma_{SSE}=\sum_{i=1}^{n}(\xi_p-\xi_e)^2 \tag{20}$$

where ξ_p is the predicted value of the model and ξ_e is the experimental value.

3. Results and discussion

3.1. Adsorbent characterization

The characteristics of HA and FA are shown in Fig. 1. The bands are similar for both acids. The 3300 cm^{-1} bands correspond to the O-H functional groups stretching for either HA and FA. Whereas the HA presents a band at 2900 corresponding to aliphatic C-H stretching the FA does not present such a band. The 1650 cm^{-1} band indicates the presence of amide 1 band (CO stretching of amid groups). At 1420 cm^{-1} the band correspond to COO- antisymmetric stretching. The 1230 cm^{-1} bands correspond to tension C-O and deformation O-H of carboxyls, phenols, esters, and aromatic 120 ethers (amide bands III).

3.2. Breakthrough curves

The effects of the presence of organic matter on the breakthrough curves is shown in Fig. 2 for the WOM, HA, and FA treatments. As is observed, the error bars for the HA and FA treatments are bigger than for the WOM treatment. This is because HA and FA

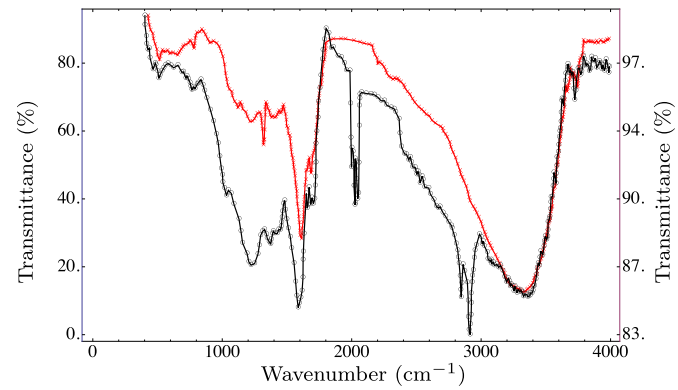

Fig. 1. Characteristics of HA and FA used for the experiments. The red -×- line represents FA (left vertical axis), and the black -∘- line represents HA (right vertical axis). (For interpretation of the references to color in this figure legend, the reader is referred to the Web version of this article.)

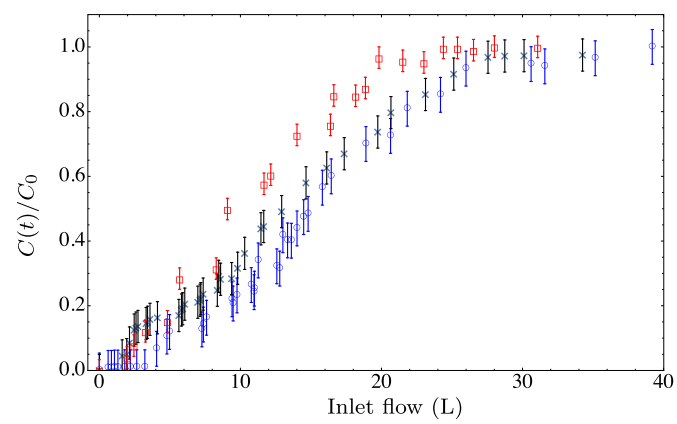

Fig. 2. Experimental breakthrough curves of the presence of organic matter on the adsorption process of As(V) on GFH. Blue −∘− represent the WOM treatment, red −□− the HA treatment, and black −×− the FA treatment. (For interpretation of the references to color in this figure legend, the reader is referred to the Web version of this article.)

introduce uncertainties to the colorimetric method used for measuring the As(V) concentration. For the WOM treatment the concentration rate of the effluent with respect to the initial concentration is less than 5% (breakthrough volume) during the first 1876 bed volumes. For the HA and FA treatments the breakthrough volume is obtained at 858 and 724 bed volumes, respectively. For the HA treatment, saturation is achieved faster during the adsorption process, and the breakthrough volume decreases with respect to the WOM treatment. For the FA treatment, the breakthrough volume decreases with respect to the WOM and HA treatments, and the breakthrough volume is reached at 26.24 L.

Table 2 shows the characteristics of the breakthrough curves. The reduction of V_r and q can be attributed to the competition of

Table 2
Characteristics of the breakthrough curve.

Parameter	WOM	HA	FA
$\%_R$	49.56	45.1	49.3
V_e (L)	38.92	30.65	33.99
q (mm mg^{-1})	6.07	4.92	5.31
V_r (L)	3.19	1.46	1.23
V_s (L)	31.73	22.43	26.24
Z_m (mm)	5.4	5.6	5.7

organic matter with As(V) for the adsorption sites on the GFH, and to the formation of complexes between organic matter and arsenic. Thus, the presence of organic matter has a critical impact on the adsorption of As(V) on the GFH filter. The maximum adsorption capacity for the WOM treatment is 6.07 mg-As(V) mg^{-1}-GFH using a concentration of 0.8 mg-As(V) L^{-1}, a bed of 6 mm tall, and a volumetric flow rate of 0.66 mL min^{-1}. When organic matter is added, the maximum adsorption capacity decreases to 5.31 and 4.92 mg-As(V) mg^{-1}-GFH for the FA and HA treatments, respectively. Also, it can be observed that the presence of organic matter leads to a reduction in the saturation volume and an increase in the length of the transfer zone.

The design of a mini-column for the adsorption of arsenic requires a prediction of the breakthrough curve for the effluent (Han et al., 2009). Several mathematical models have been developed in order to describe the performance of mini-columns for different applications (Kumar and Chakraborty, 2009; Han et al., 2009; Vinodhini and Das, 2010; Chen et al., 2012). In the present study, the Belter, Thomas, and HSD models are applied in order to identify the best model that predicts the performance of the dynamic adsorption of arsenic in mini-columns, as well as to predict information that can be obtained only by designing complex and expensive experiments.

Fig. 3 shows the prediction of the breakthrough curves obtained using the Belter, Thomas, and HSD models. The model parameters and correlation coefficients obtained from the analysis of the breakthrough curves for all treatments and different models are shown in Table 3. It can be observed that the models predict well the experiments. For the HA treatment, the Belter model provides a correlation coefficient of $R^2 > 0.989$, and the Thomas model provides a correlation coefficient of $R^2 > 0.988$. For the FA treatment, the Belter model provides a correlation coefficient of $R^2 > 0.995$, and the Thomas model provides a correlation coefficient of $R^2 > 0.987$. For the HSD model, the error is lower than 0.6 for the three treatments using a collocation method with 10 collocation points in the Z and R directions. The number of collocation points do not alter the final result for the HSD model since a variation in the results of only 0.1% is obtained when adding more than 10 collocation points.

The parameter V_m used in the Belter model (see Table 3) for the adsorption of As(V) on GFH shows that the WOM treatment handles a bigger volume before the effluent concentration is 50% of that of the influent. Also, the adsorption capacity, q, of the Thomas model is reduced when organic matter is added to the treatment. These results are in agreement with the results obtained from the experiments.

The HSD model predicts well the behavior of the breakthrough curves, as is shown in Fig. 3c. The presence of organic matter tends to reduce D_g, implying that the affinity of the As(V) is reduced as organic matter is introduced to the influent. The affinity of As(V) has its lowest value in presence of FA. Bi decreases as FA are added to the influent, which suggests that in the absence of FA, the intraparticle mass transfer and the liquid-phase mass transfer are balanced. However, as organic matter is added to the influent, the intraparticle mass transfer controls the adsorption rate. Also, when HA are added to the influent, the liquid-phase mass transfer becomes more dominant in the adsorption rate. In addition, when HA

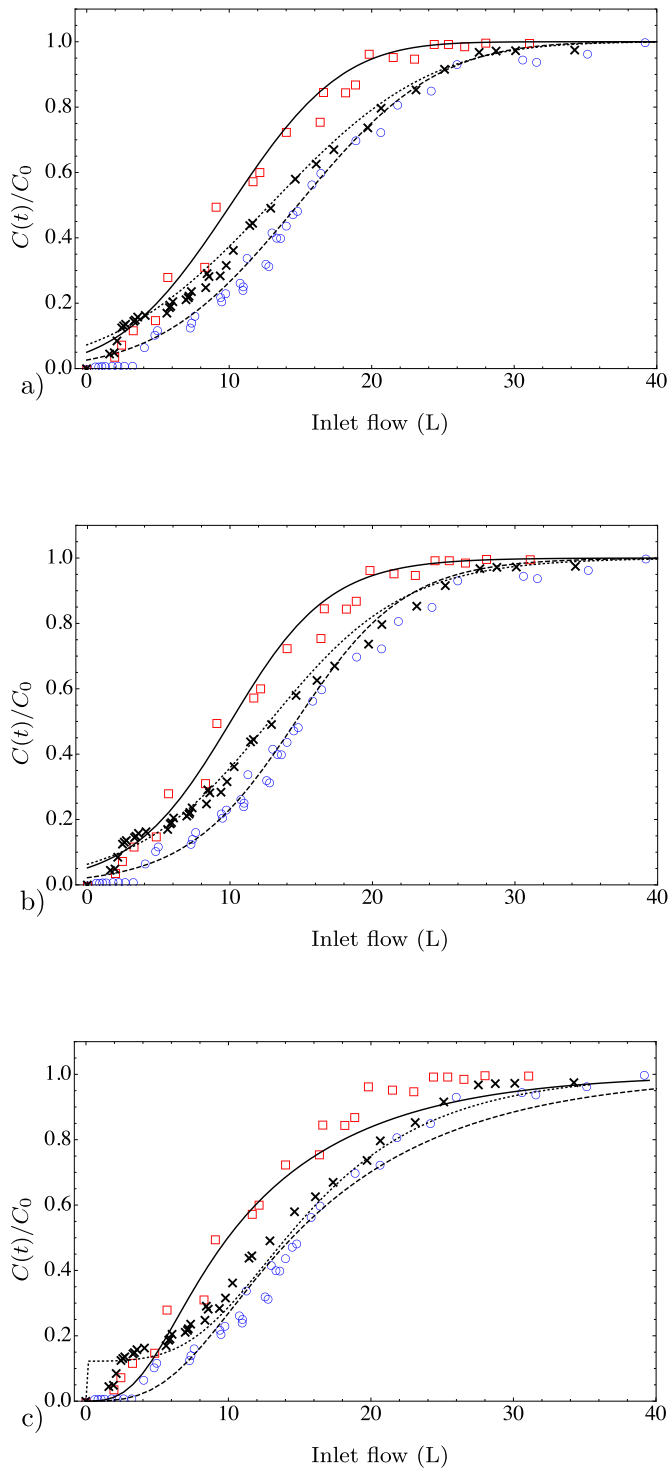

Fig. 3. Numerical prediction of the Breakthrough curves using the a) Belter, b) Thomas, and c) HSD models. Marks represent experimental data (see Fig. 2), and lines represent the numerical approximation.

Table 3
Parameters used for the numerical modeling of breakthrough curves.

Treatment	Belter Model			Thomas Model			HSD Model		
	V_m(L)	σ	R^2	k_T(10^{-4}L $mg^{-1}min^{-1}$)	q(mg g^{-1})	R^2	Bi	St	D_g
WOM	14.810	0.515	0.992	2.14	5.85	0.990	1.5	3.5	4120
HA	10.082	0.608	0.989	2.38	4.02	0.988	1.9	3.5	3000
FA	12.842	0.686	0.995	1.74	5.11	0.987	0.9	0.7	810

are added to the influent, the HSD model predicts a smaller mass transfer zone for the WOM treatment, and when FA are added to the influent, the model predicts an increase in the length of the mass transfer zone.

Fig. 4 shows the behavior of the dimensionless solid-phase concentration for three selected times, i.e., at the beginning ($t = 0$), at an intermediate time ($t = \frac{1}{2}\, t_{\max}$), and at saturation ($t = t_{\max}$). The x–axis represents the position from the center of the solid phase. For the WOM treatment, the surface of the solid phase is almost saturated at an intermediate time, whereas the center only contains 0.7 of the final concentration. For the HA treatment, the solid-phase is almost saturated at all times, implying that when organic matter is added the adsorbent reaches saturation faster than for the WOM treatment. For the FA treatment, the model shows that when the surface reaches the 0.7 of the final concentration the center is still at 0.38. These results suggest that the FA are moved by diffusion at a lower ratio than the HA.

3.3. pH behavior

The influent pH is set to 7.4 for all treatments. Fig. 5 shows the pH behavior of the effluent for the WOM, HF, and AF treatments. For the WOM treatment, when water passes through the filter, the pH decreases to approximately a value of 4; then, the pH increases until the breakthrough volume reaches equilibrium at a pH of approximately 9. For the HA treatment, the increase in pH reaches equilibrium when saturation is reached. For the FA treatment, the increase in pH reaches equilibrium at the mass transfer zone. The figure also shows that the presence of organic matter significantly influence the pH behavior, decreasing the slope of the pH curve. This suggests that organic matter act as a buffer, decreasing the variation effect of the effluent's pH. The initial pH at equilibrium decreases because the concentration of chlorine is increasing, as is explained in Paterson and Rahman (1983). A low pH increases the positive charge on the surface of GFH causing an increase of the attraction forces. This effect is not noticeable because the pH is adjusted to compensate for the liberation of protons from the GFH surface due to the charge difference produced by the Cl-ions liberated to the solution.

3.4. Desorption efficiency

The desorption efficiency for the three treatments is shown in Table 4. These efficiencies are obtained by calculating the ratio of the total amount of As(V) desorbed and the total amount of As(V) adsorbed in the column. The desorption efficiency is in the range of 84.88–99.38%. The WOM treatment presents the lowest As(V) desorption efficiency (84.88%), the FA column presents the highest As(V) desorption efficiency (99.38%), and the HA shows an As(V) desorption efficiency of 92.00%. This is in agreement with the fact that arsenic is more stable in association with FA at neutral pH (Mandal et al., 2013), but is more easily bounded to HA (Fakour and Lin, 2014). These results are consistent with the desorption energies reported in the literature (4.429 kJ mol^{-1} for FA, 6.421 kJ mol^{-1} for HA, and 7.480 kJ mol^{-1} for WOM).

The desorption of arsenic is affected by the presence of organic matter, especially for the presence of FA which shows a value of 99.38%. This evidence suggest that the adsorption bounds are stronger in the absence of organic matter, and the adsorption mechanism is weaker in the presence of organic matter. This behavior is observed because, as proposed by the Dubinin-Radushkevi model (Dubinin and Radushkevich, 1947), the adsorption energy is lower when organic matter is added; that is, organic matter lowers the bound energy, which is reflected in a higher desorption efficiency.

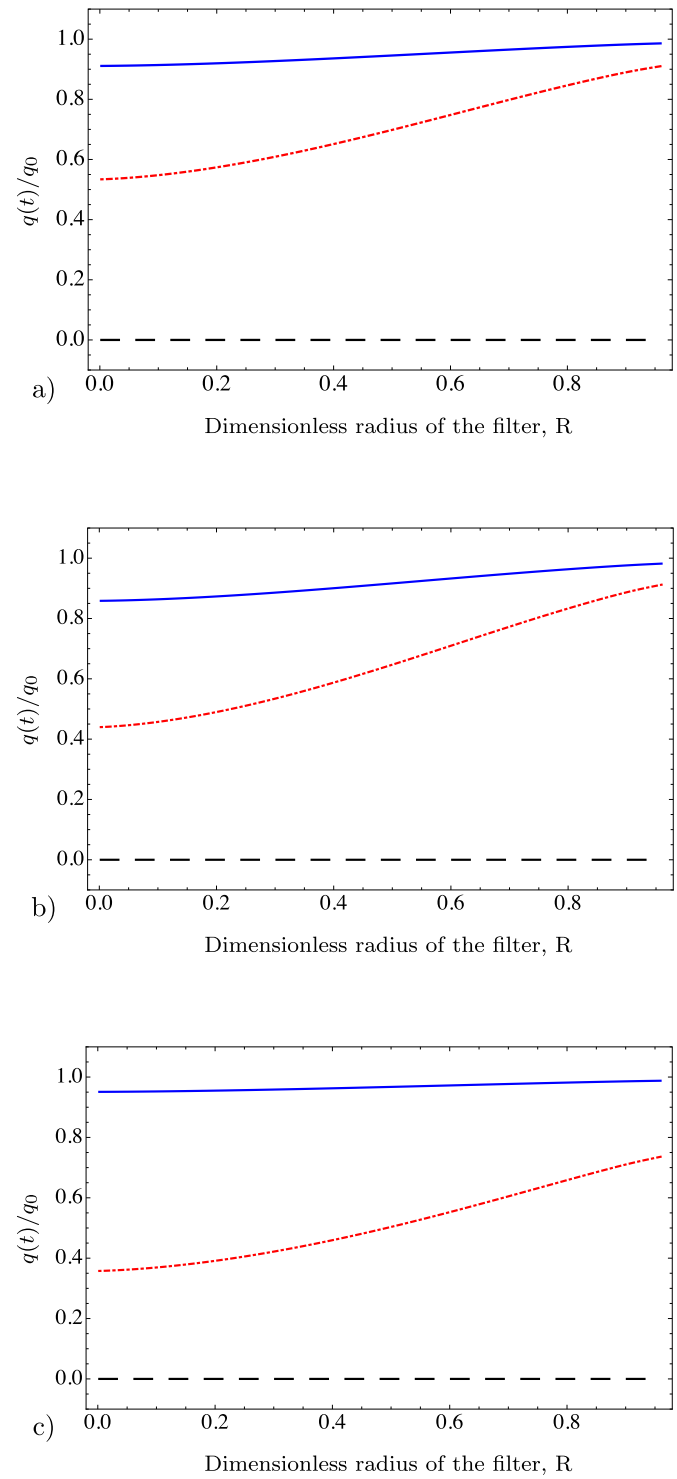

Fig. 4. Numerical solid-phase curves obtained for the a) WOM, b) HA, and c) FA treatments using the HSD model. The dashed black line represents the initial concentration ($t = 0$), the dotted red line represents the concentration at an intermediate time ($t = \frac{1}{2}t_{\max}$), and the continuous blue line represents the concentration at saturation ($t = t_{\max}$). (For interpretation of the references to color in this figure legend, the reader is referred to the Web version of this article.)

Fig. 6 and Table 4 show that in the WOM treatment the As(V) is strongly retained as opposed to those treatments with organic matter. These results are in agreement with those reported previously in the literature for GFH by Joshi and Chaudhuri (1996) and Jackson and Miller (2000).

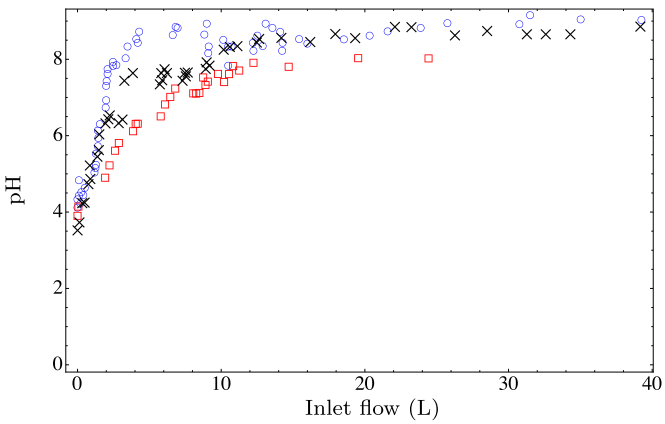

Fig. 5. Experimental pH profile for the WOM (blue –∘–), HA (red –□–), and FA (black –×–) treatments. (For interpretation of the references to color in this figure legend, the reader is referred to the Web version of this article.)

Table 4
Experimental values for the As(V) desorption efficiency in the mini-columns.

Treatment	Desorption Efficiency (%)
WOM	84.88 ± 0.03763
HA	92.00 ± 0.03781
FA	99.38 ± 0.04150

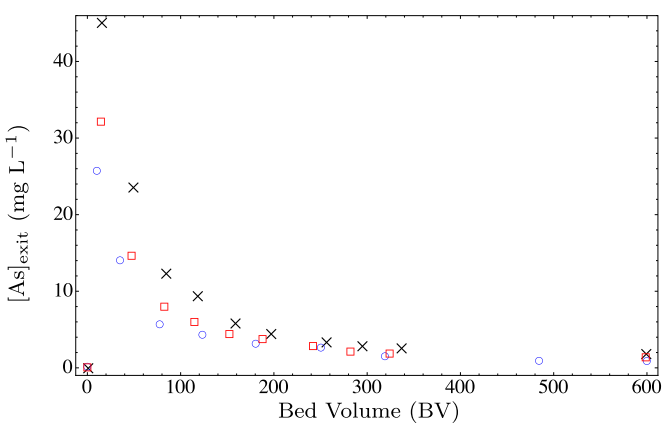

Fig. 6. Experimental As(V) desorption curves for the WOM (blue –∘–), HA (red –□–), and FA (black –×–) treatments. (For interpretation of the references to color in this figure legend, the reader is referred to the Web version of this article.)

3.5. Other findings

As a complement to the study, dissolved Fe is quantified using the 3500-Fe-D phenantroline standard method. The detection limits of this method are 0.2–10 mg L^{-1}. None of the samples presents dissolved Fe. The samples show Fe levels lower than 0.3 mg L^{-1}, which is the permissible limit by the Mexican Official Norm NOM-127-SSA1-1994 (DOF-MX, 1994). In addition, results show that GFH can be regenerated and reused if desired, although a detailed analysis of the reuse of GFH is currently in progress.

The present work complements those by Saldana-Robles et al. (2017) and Li et al. (2017) by providing experimental breakthrough, desorption, and pH curves, as well as numerical predictions of adsorption of As(V) on GFH.

4. Conclusions

In this work the impact of organic matter on the removal procedure of As(V) using GFH in mini-columns is presented. The study finds that the treatments with FA and HA decrease the saturation volume, increase the transfer zone, and decrease both the adsorption capacity and the breakthrough volume. The pH curves are reduced to a value close to 4 and reach a plateau at about 8 for all treatments; also, the HA treatment shows the lowest pH. The FA treatment shows a higher As(V) desorption efficiency than the HA and WOM treatments, and the HA treatment shows a higher desorption efficiency than the WOM treatment. In addition, there is no evidence of diluted *Fe* in the effluent. The Thomas and Belter models provide a good fit for all treatments, although the Thomas model overestimates the adsorption capacity when compared to experimental results. The HSD model fits reasonably well the experiments and provides detailed information about the concentration of As(V) in both the liquid and solid phases. The results obtained with the HSD model indicate that for the HA treatment the solid phase is saturated homogeneously, whereas for the WOM and FA treatments the center of the solid phase is saturated at a slower rate, being the FA the slowest of the three treatments. The findings provide key information for the fabrication of efficient water filters to tackle the problem of contamination of groundwater with arsenic in order to supply clean water to a society, contributing to the sustainability of the Bajio region in Mexico.

Acknowledgements

A. Saldaña-Robles, N. Saldaña-Robles, A.L. Saldaña-Robles thank to the Office of Innovation, Science, and Higher Education (SICES) of the state of Guanajuato, and to the CIATEC for financial support. C.E. Damian-Ascencio and S. Cano-Andrade gratefully acknowledge to the National Council of Science and Technology (CONACyT), Mexico, for financial support under the SNI program.

Nomenclature

Acronyms

GFH	Granular Ferric Hydroxide
WOM	Without Organic Matter
HA	Humic Acids
FA	Fulvic Acids
HSD	Homogeneous Surface Diffusion
TOC	Total Dissolved Organic Carbon

Symbols

η_{reg}	Regeneration efficiency
m	Mass of the adsorbent
m_{ad}	Total mass of arsenic adsorbed at saturation
m_{des}	Total mass of arsenic that is desorbed
m_{tot}	Total mass of arsenic stored in the column
m_{dry}	Dry mass of the adsorbent in the column
$C(t)$	Concentration of arsenic in the effluent
C_0	Concentration of arsenic in the influent
C_0^*	Concentration of arsenic at the adsorbent's surface
Z_m	Mass transfer zone
z	Column height
V_r	Breakthrough volume
V_s	Saturation volume
V_e	Volume of the effluent
V_b	Bed volume
V_m	Effluent volume at which half of C_0 is obtained

Q	Volumetric flow of the influent
t_s	Saturation time
$\%_R$	Percentage of arsenic removal
t_e	Empty bed contact time
σ	Standard deviation
q	Adsorption capacity
$q_{\max}$	Maximum adsorption capacity in the column
u	Velocity of the influent
k_T	Kinetic constant of the Thomas model
D_g	Solute distribution parameter
X	Dimensionless liquid-phase concentration
X^*	Dimensionless liquid-phase concentration at the adsorbent's surface
Y	Dimensionless solid-phase concentration
Z	Dimensionless axial coordinate
T	Dimensionless time
R	Dimensionless radius
t	Time
r_p	Radius of the adsorbent
p	Solid-phase concentration
p_0	Solid-phase concentration at equilibrium
Bi	Biot number
Γ_{SSE}	Sum square error

References

Alarcón-Herrera, M.T., Bundschuh, J., Nath, B., Nicolli, H.B., Gutierrez, M., Reyes-Gomez, V.M., Nunez, D., Martín-Dominguez, I.R., Sracek, O., 2013. Co-occurrence of arsenic and fluoride in groundwater of semi-arid regions in Latin america: genesis, mobility and remediation. J. Hazard Mater. 262, 960–969.

Amy, G.L., Chen, H.W., Dinzo, A., Brandhuber, P., 2005. Adsorbent Treatment Technologies for Arsenic Removal. American Water Works Association.

Anawar, H.M., Tareq, S.M., Ahmed, G., 2013. Is organic matter a source or redox driver or both for arsenic release in groundwater? Phys. Chem. Earth, Parts A/B/C 49–56.

Arcega-Cabrera, F., Fargher, L.F., 2016. Education, fish consumption, well water, chicken coops, and cooking fires: using biogeochemistry and ethnography to study exposure of children from yucatan, Mexico to metals and arsenic. Sci. Total Environ. 568, 75–82.

Aredes, S., Klein, B., Pawlik, M., 2012. The removal of arsenic from water using natural iron oxide minerals. J. Clean. Prod. 29, 208–213.

Armienta, M.A., Segovia, N., 2008. Arsenic and fluoride in the groundwater of Mexico. Environ. Geochem. Health 30, 345–353.

Armienta, M.A., Talavera, O., Morton, O., Barrera, M., 2003. Geochemistry of metals from mine tailings in taxco, Mexico. Bull. Environ. Contam. Toxicol. 71, 0387–0393.

Ayoob, S., Gupta, A.K., Bhakat, P.B., 2007. Analysis of breakthrough developments and modeling of fixed bed adsorption system for as (v) removal from water by modified calcined bauxite (mcb). Separ. Purif. Technol. 52, 430–438.

Baig, S.A., Zhu, J., Tan, L., Xue, X., Sun, C., Xu, X., 2014. Influence of calcination on magnetic honeycomb briquette cinders composite for the adsorptive removal of as (iii) in fixed-bed column. Chem. Eng. J. 257, 1–9.

Brammer, H., Ravenscroft, P., 2009. Arsenic in groundwater: a threat to sustainable agriculture in south and south-east asia. Environ. Int. 35, 647–654.

Bulut, G., Yenial, U., Emiroglu, E., Sirkeci, A.A., 2014. Arsenic removal from aqueous solution using pyrite. J. Clean. Prod. 84, 526–532.

Burgess, W.G., Hoque, M.A., Michael, H.A., Voss, C.I., Breit, G.N., Ahmed, K.M., 2010. Vulnerability of deep groundwater in the bengal aquifer system to contamination by arsenic. Nat. Geosci. 3, 83–87.

Buschmann, J., Kappeler, A., Lindauer, U., Kistler, D., Berg, M., Sigg, L., 2006. Arsenite and arsenate binding to dissolved humic acids: influence of ph, type of humic acid, and aluminum. Environ. Sci. Technol. 40, 6015–6020.

Chen, S., Yue, Q., Gao, B., Li, Q., Xu, X., Fu, K., 2012. Adsorption of hexavalent chromium from aqueous solution by modified corn stalk: a fixed-bed column study. Bioresour. Technol. 113, 114–120.

Chu, K.H., 2004. Improved fixed bed models for metal biosorption. Chem. Eng. J. 97, 233–239.

Chu, K.H., 2014. Prediction of arsenic breakthrough in a pilot column of polymer-supported nanoparticles. J. Water Process Eng. 3, 117–122.

Cullen, W.R., Reimer, K.J., 1989. Arsenic speciation in the environment. Chem. Rev. 89, 713–764.

Daus, B., Wennrich, R., Weiss, H., 2004. Sorption materials for arsenic removal from water: a comparative study. Water Res. 38, 2948–2954.

Dubinin, M.M., Radushkevich, L.V., 1947. Equation of the characteristic curve of activated charcoal. Chem. Zentr. 1, 875.

Fakour, H., Lin, T.F., 2014. Experimental determination and modeling of arsenic complexation with humic and fulvic acids. J. Hazard Mater. 279, 569–578.

Diario oficial de la Federación, 1994. Nom-127-SSA1–1994, Salud ambiental, agua para uso y consumo humano. límites permisibles de calidad y tratamiento que debe someterse el agua para su potabilización. DOF-MX, pp. 108–112.

Genc-Fuhrman, H., Mikkelsen, P.S., Ledin, A., 2016. Simultaneous removal of as, cd, cr, cu, ni and zn from stormwater using high-efficiency industrial sorbents: effect of ph, contact time and humic acid. Sci. Total Environ. 566, 76–85.

Genz, A., Baumgarten, B., Goernitz, M., Jekel, M., 2008. Nom removal by adsorption onto granular ferric hydroxide: equilibrium, kinetics, filter and regeneration studies. Water Res. 42, 238–248.

Ghosh, A., Chakrabarti, S., Ghosh, U.C., 2014. Fixed-bed column performance of mn-incorporated iron (iii) oxide nanoparticle agglomerates on as (iii) removal from the spiked groundwater in lab bench scale. Chem. Eng. J. 248, 18–26.

Han, R., Zou, L., Zhao, X., Xu, Y., Xu, F., Li, Y., Wang, Y., 2009. Characterization and properties of iron oxide-coated zeolite as adsorbent for removal of copper (ii) from solution in fixed bed column. Chem. Eng. J. 149, 123–131.

Hand, D.W., Crittenden, J.C., Thacker, W.E., 1984. Simplified models for design of fixed-bed adsorption systems. J. Environ. Eng. 110, 440–456.

Hu, X., Ding, Z., Zimmerman, A.R., Wang, S., Gao, B., 2015. Batch and column sorption of arsenic onto iron-impregnated biochar synthesized through hydrolysis. Water Res. 68, 206–216.

Iakovleva, E., Maydannik, P., Ivanova, T.V., Sillanpaa, M., Tang, W.Z., Makila, E., Salonen, J., Gubal, A., Ganeev, A.A., Kamwilaisak, K., Wang, S., 2016. Modified and unmodified low-cost iron-containing solid wastes as adsorbents for efficient removal of as(iii) and as(v) from mine water. J. Clean. Prod. 133, 1095–1104.

Jackson, B.P., Miller, W.P., 2000. Effectiveness of phosphate and hydroxide for desorption of arsenic and selenium species from iron oxides. Soil Sci. Soc. Am. J. 64, 1616–1622.

Joshi, A., Chaudhuri, M., 1996. Removal of arsenic from ground water by iron oxide-coated sand. J. Environ. Eng. 122, 769–771.

Kofa, G.P., NdiKoungou, S., Kayem, G.J., Kamga, R., 2015. Adsorption of arsenic by natural pozzolan in a fixed bed: determination of operating conditions and modeling. J. Water Process Eng. 6, 166–173.

Kong, Y., Kang, J., Shen, J., Chen, Z., Fan, L., 2017. Influence of humic acid on the removal of arsenate and arsenic by ferric chloride: effects of ph, as/fe ratio, initial as concentration, and co-existing solutes. Environ. Sci. Pollut. Control Ser. 24, 2381–2393.

Kumar, P.A., Chakraborty, S., 2009. Fixed-bed column study for hexavalent chromium removal and recovery by short-chain polyaniline synthesized on jute fiber. J. Hazard Mater. 162, 1086–1098.

Kundu, S., Gupta, A.K., 2007. As (iii) removal from aqueous medium in fixed bed using iron oxide-coated cement (iocc): experimental and modeling studies. Chem. Eng. J. 129, 123–131.

Li, F., Guo, H., Zhou, X., Zhao, K., Shen, J., Liu, F., Wei, C., 2017. Impact of natural organic matter on arsenic removal by modified granular natural siderite: evidence of ternary complex formation by hpsec-uv-icp-ms. Chemosphere 168, 777–785.

Luo, C., Xie, Y., Li, F., Jiang, T., Wang, Q., Jiang, Z., Wei, S., 2015. Adsorption of arsenate on iron oxides as influenced by humic acids. J. Environ. Qual. 44, 1729–1737.

Maji, S.K., Pal, A., Pal, T., 2008. Arsenic removal from real-life groundwater by adsorption on laterite soil. J. Hazard Mater. 151, 811–820.

Mandal, S.K., Ray, R., Chowdhury, C., Majumder, N., Jana, T.K., 2013. Implication of organic matter on arsenic and antimony sequestration in sediment: evidence from sundarban mangrove forest, India. Bull. Environ. Contam. Toxicol. 90, 451–455.

Masindi, V., Gitari, W.M., 2016. Removal of arsenic from wastewaters by cryptocrystalline magnesite: complimenting experimental results with modelling. J. Clean. Prod. 113, 318–324.

Mehta, V.S., Chaudhari, S.K., 2015. Arsenic removal from simulated groundwater using household filter columns containing iron filings and sand. J. Water Process Eng. 6, 151–157.

Mendoza-Amézquita, E., Armienta-Hernández, M.A., Ayora, C., Soler, A., Ramos-Ramírez, E., 2006. Potencial lixiviación de elementos traza en jales de las minas la asunción y las torres, en el distrito minero de guanajuato, méxico. Rev. Mex. Ciencias Geol. 23, 75–83.

Nguyen, V.L., Chen, W.H., Young, T., Darby, J., 2011. Effect of interferences on the breakthrough of arsenic: rapid small scale column tests. Water Res. 45, 4069–4080.

Nieto-Delgado, C., Rangel-Mendez, J.R., 2012. Anchorage of iron hydro (oxide) nanoparticles onto activated carbon to remove as (v) from water. Water Res. 46, 2973–2982.

Ongley, L.K., Sherman, L., Armienta, A., Concilio, A., Salinas, C.F., 2007. Arsenic in the soils of zimapán, Mexico. Environ. Pollut. 145, 793–799.

Paterson, R., Rahman, H., 1983. The ion exchange properties of crystalline inorganic oxide-hydroxides: Part i. βfeooh: a variable capacity anion exchanger. J. Colloid Interface Sci. 94, 60–69.

Rahman, M.S., Whalen, M., Gagnon, G.A., 2013. Adsorption of dissolved organic matter (dom) onto the synthetic iron pipe corrosion scales (goethite and magnetite): effect of ph. Chem. Eng. J. 234, 149–157.

Razo, I., Carrizales, L., Castro, J., Díaz-Barriga, F., Monroy, M., 2004. Arsenic and heavy metal pollution of soil, water and sediments in a semi-arid climate mining area in Mexico. Water, Air, Soil Pollut. 152, 129–152.

Redman, A.D., Macalady, D.L., Ahmann, D., 2002. Natural organic matter affects arsenic speciation and sorption onto hematite. Environ. Sci. Technol. 36, 2889–2896.

Romero, F.M., Armienta, M.A., Villaseñor, G., González, J.L., 2006. Mineralogical constraints on the mobility of arsenic in tailings from zimapán, hidalgo, Mexico. Int. J. Environ. Pollut. 26, 23–40.
Saldana-Robles, A., Saldana-Robles, N., Saldana-Robles, A.L., Damian-Ascencio, C., Rangel-Hernandez, V.H., Guerra-Sanchez, R., 2017. Arsenic removal from aqueous solutions and the impact of humic and fulvic acids. J. Clean. Prod. 159, 425–431.
Santos-Jallath, J., Castro-Rodríguez, A., Huezo-Casillas, J., Torres-Bustillos, L., 2012. Arsenic and heavy metals in native plants at tailings impoundments in queretaro, Mexico. Phys. Chem. Earth, Parts A/B/C 37, 10–17.
Tang, W.W., Zeng, G.M., Gong, J.L., Liang, J., Xu, P., Zhang, C., Huang, B.B., 2014. Impact of humic/fulvic acid on the removal of heavy metals from aqueous solutions using nanomaterials: a review. Sci. Total Environ. 468, 1014–1027.
Tareq, S.M., Maruo, M., Ohta, K., 2013. Characteristics and role of groundwater dissolved organic matter on arsenic mobilization and poisoning in Bangladesh. Phys. Chem. Earth, Parts A/B/C 77–84.
Thomas, H.C., 1944. Heterogeneous ion exchange in a flowing system. J. Am. Chem. Soc. 66, 1664–1666.
Tresintsi, S., Simeonidis, K., Vourlias, G., Stavropoulos, G., Mitrakas, M., 2012. Kilogram-scale synthesis of iron oxy-hydroxides with improved arsenic removal capacity: study of fe (ii) oxidation-precipitation parameters. Water Res. 46, 5255–5267.
Trois, C., Cibati, A., 2015. South african sands as a low cost alternative solution for arsenic removal from industrial effluents in permeable reactive barriers: column tests. Chem. Eng. J. 259, 981–989.
Uwamariya, V., Petrusevski, B., Slokar, Y.M., Aubry, C., Lens, P.N.L., Amy, G.L., 2015. Effect of fulvic acid on adsorptive removal of cr(vi) and as(v) from groundwater by iron oxide-based adsorbents. Water Air Soil Pollut. 226, 184.
Vinodhini, V., Das, N., 2010. Packed bed column studies on cr (vi) removal from tannery wastewater by neem sawdust. Desalination 264, 9–14.
Watanabe, C.H., Monteiro, A.S.C., Gontijo, E.S.J., Lira, V.S., Bueno, C.d.C., Kumar, N.T., Fracacio, R., Rosa, A.H., 2017. Toxicity assessment of arsenic and cobalt in the presence of aquatic humic substances of different molecular sizes. Ecotoxicol. Environ. Saf. 139, 1–8.
Wurl, J., Mendez-Rodriguez, L., Acosta-Vargas, B., 2014. Arsenic content in groundwater from the southern part of the san antonio-el triunfo mining district, baja California sur, Mexico. J. Hydrol. 518, 447–459.
Yin, H., Kong, M., Gu, X., Chen, H., 2017. Removal of arsenic from water by porous charred granulated attapulgite-supported hydrated iron oxide in bath and column modes. J. Clean. Prod. 166, 88–97.